

From fabrication to mode mapping in silicon nitride microdisks with embedded colloidal quantum dots

Bram De Geyter, Katarzyna Komorowska, Edouard Brainis, Philippe Emplit, Pieter Geiregat et al.

Citation: *Appl. Phys. Lett.* **101**, 161101 (2012); doi: 10.1063/1.4758990

View online: <http://dx.doi.org/10.1063/1.4758990>

View Table of Contents: <http://apl.aip.org/resource/1/APPLAB/v101/i16>

Published by the [American Institute of Physics](http://www.aip.org).

Related Articles

Laser irradiation effects on the CdTe/ZnTe quantum dot structure studied by Raman and AFM spectroscopy
J. Appl. Phys. **112**, 063520 (2012)

Single photon emission in the red spectral range from a GaAs-based self-assembled quantum dot
Appl. Phys. Lett. **101**, 103108 (2012)

Structural characterization of CdSe/ZnS quantum dots using medium energy ion scattering
Appl. Phys. Lett. **101**, 023110 (2012)

The conduction band absorption spectrum of interdiffused InGaAs/GaAs quantum dot infrared photodetectors
J. Appl. Phys. **111**, 123719 (2012)

Site-controlled formation of InAs/GaAs quantum-dot-in-nanowires for single photon emitters
Appl. Phys. Lett. **100**, 263101 (2012)

Additional information on *Appl. Phys. Lett.*

Journal Homepage: <http://apl.aip.org/>

Journal Information: http://apl.aip.org/about/about_the_journal

Top downloads: http://apl.aip.org/features/most_downloaded

Information for Authors: <http://apl.aip.org/authors>

ADVERTISEMENT

The advertisement for Physical Review X (PRX) is a horizontal banner. On the left, a blue vertical bar contains the text 'AMERICAN PHYSICAL SOCIETY'S OPEN ACCESS JOURNAL' in white, all-caps font. To the right of this bar, the background is a dark, abstract image with a glowing red and orange light source on the right side. The letters 'PRX' are prominently displayed in a large, white, serif font. To the right of 'PRX' is a stylized white logo consisting of two overlapping, curved lines that form a shape resembling a double helix or a quantum symbol. Further to the right, the text 'Committed to Excellence' is written in a white, sans-serif font. Below this, 'Physical Review X' is written in a smaller white font, followed by the website address 'prx.aps.org'.

From fabrication to mode mapping in silicon nitride microdisks with embedded colloidal quantum dots

Bram De Geyter,^{1,2,3} Katarzyna Komorowska,^{1,3} Edouard Brainis,⁴ Philippe Emplit,⁴ Pieter Geiregat,^{1,2,3} Antti Hassinen,^{2,3} Zeger Hens,^{2,3} and Dries Van Thourhout^{1,3,a)}

¹Photonics Research Group, INTEC Department, Ghent University-IMEC, Sint-Pietersnieuwstraat 41, 9000 Ghent, Belgium

²Department of Inorganic and Physical Chemistry, Ghent University, Krijgslaan 281 (S3), B-9000 Ghent, Belgium

³Center for Nano- and Biophotonics (NB-Photonics), Ghent University, 9000 Ghent, Belgium

⁴Service OPERA, Université Libre de Bruxelles (ULB), Brussels, Belgium

(Received 21 June 2012; accepted 28 September 2012; published online 15 October 2012)

We report on the fabrication of free-standing and optically active microdisks with cadmium-based colloidal quantum dots embedded directly into silicon nitride. We show that the process optimization results in low-loss silicon nitride microdisks. The Si_3N_4 matrix provides the stability necessary to preserve the optical properties of the quantum dots and observe efficient coupling of the photoluminescence to the resonating microdisk modes. Using a spectrally and spatially resolved microphotoluminescence measurement, we map the emission pattern from the microdisk. This technique allows us to identify the resonant modes. The results show good agreement with numerical mode simulations. © 2012 American Institute of Physics. [<http://dx.doi.org/10.1063/1.4758990>]

The recent progress in the synthesis of solution processable quantum dots (QDs) has sprouted significant interest to use these materials in solar cells, bio-imaging, and integrated photonics.¹ Easy control over their size, shape, composition, concentration, and surface chemistry allows efficient engineering of their optical and electrical properties, tailored to the application. Moreover, their inherent quantum mechanical nature makes their interaction with a quantized optical field interesting from a fundamental viewpoint, making cavity-quantum electrodynamics easily accessible using wet processing techniques, such as spincoating, dropcasting, and layer-by-layer deposition.^{2,3}

Since colloidal QDs are synthesized using wet chemistry techniques, most studies of the fundamental photophysical properties are carried out in solution or on thin films. However, as the field becomes more application oriented, a need arises to embed them in a solid matrix that adds both stability and functionality. More specifically, combining these QDs with integrated photonic circuits to form lasers, modulators, and other nonlinear components will require a platform technology. This platform should be able to provide the necessary optical components, such as waveguides, gratings, and resonators and allow for a stable and efficient integration of the active materials over a broad wavelength range. A material system ideally suited to fulfill all these requirements is silicon nitride (Si_3N_4). It is a high index material ($n = 1.8\text{--}2.2$), commonly used in the CMOS (complementary metal-oxide-semiconductor) industry for its excellent electrical and chemical isolation of sensitive components. Moreover, as an insulator, it is transparent in both the visible and near-infrared spectral region, providing a versatile platform for both cadmium and lead-based colloidal QDs or future material systems yet to be developed.

Several authors have reported on the coupling of QD emission to optical microcavities.^{2,4–17} Most often the cavity is a glass microsphere or capillary, where QDs are neither embedded into the resonator material closest to the whispering gallery modes (WGM) nor does the technology provide the possibility of coupling to other integrated optical components.

In this letter we report on the fabrication of free-standing and optically active microdisks with QDs embedded directly into Si_3N_4 . We show that the process optimization results in low-loss silicon nitride microdisks. The Si_3N_4 matrix provides the stability necessary to preserve the optical properties of the QDs and observe efficient coupling of the photoluminescence (PL) to the resonating microdisk modes. Using a spectrally and spatially resolved microphotoluminescence measurement, we are able to selectively pump parts of the microdisk and observe the radiation pattern both spatially and spectrally. Finally, we compare the observed spectra with mode solver simulations.

In the present study we focus on *giant* CdSe/14CdS QDs ($d = 12$ nm), made using successive ion layer adsorption and reaction (SILAR).¹⁸ The absorption and emission spectrum in solution is shown in Figure 1(a). We note that we obtained similar results with several other types of quantum dots and quantum rods, emitting in the visible and in the infrared (see Figures 1(b)–1(d) and supplementary material²³). We therefore stress that this fabrication procedure can be easily extended to other colloidal QD systems, both in the visible and near-infrared region of the spectrum, and thus provides a platform for studies of colloidal QDs coupled to photonic resonators.

For the microdisk fabrication, we use a standard silicon substrate, onto which an 80 nm layer of Si_3N_4 is deposited using plasma-enhanced chemical vapour deposition (PECVD). The solid Si_3N_4 is formed from a 31:28 sccm mixture of silane gas (SiH_4) and ammonia gas (NH_3). The substrate is held at 300 °C during the deposition. This results in a high-density

^{a)}Email: Dries.Vanhourhout@intec.UGent.be. URL: <http://www.photonics.intec.ugent.be>.

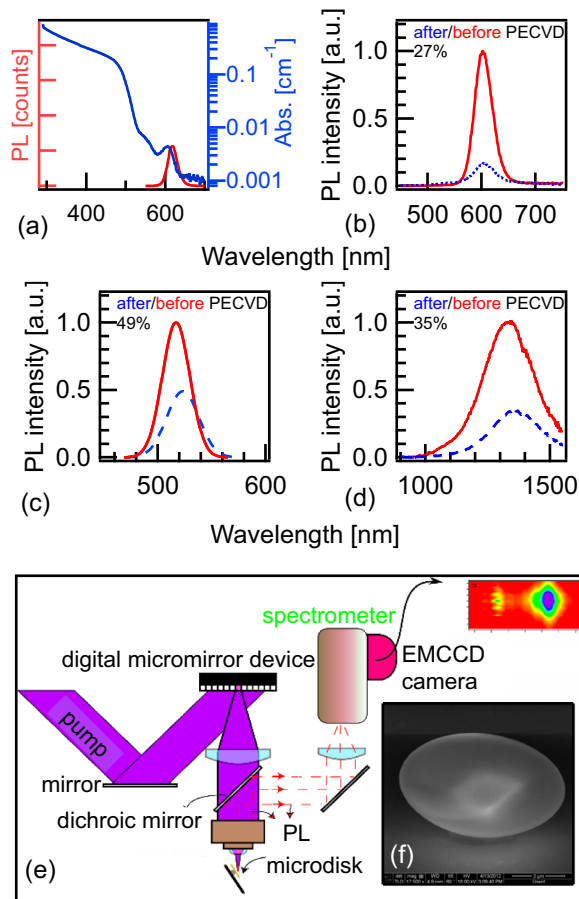


FIG. 1. (a) PL (red) and absorption (blue) spectrum of 12 nm *giant* CdSe/14CdS QDs used in the microdisk experiment shows the 12 nm Stokes shift between absorption and emission. (b) PL spectrum of spincoated CdSe/16CdS QDs before (red) and after (blue) deposition of low-index Si₃N₄ shows that 27% of the emission remains after Si₃N₄ deposition. (c) A similar experiment for CdSe/2ZnS QDs illustrates that 49% of the PL remains after deposition. (d) Also for near-infrared emitting PbS/CdS QDs 35% of the PL is recovered after Si₃N₄ deposition. (e) Scheme of the experimental setup to perform the spatial and spectral mapping of the optical modes (f) SEM picture of a typical microdisk. The silicon support pillar can be seen through the microdisk.

Si₃N₄ layer with a refractive index of 2.03 ($\lambda = 650$ nm), as measured using ellipsometry. Next the microdisk pattern is transferred to a resist spincoated on the Si₃N₄ layer using UV optical lithography and subsequently etched into the Si₃N₄ layer using reactive ion etching (RIE). Optimization of the gas mixture and processing parameters was carried out to reduce the roughness of the microdisk edge. This roughness is critical to having low-loss WGM. The optimal parameters on our RIE system were CF₄ : O₂ 30:30 sccm at 40 mTorr and 150 W. To obtain a free-standing microdisk, the silicon substrate was selectively wet-etched using a mixture of 30 g KOH and 120 ml of deionized water at 60 °C. After formation of the Si pillar, a dispersion of QDs in toluene with a volume fraction of 0.05% was spincoated at 2000 rpm over the substrate. This results in a 120 nm QD layer, as measured using scanning probe microscopy (SPM) and scanning electron microscopy (SEM). Finally, another 80 nm layer of Si₃N₄ was deposited using PECVD. This time the substrate temperature is lowered to 120 °C to reduce possible loss of the passivating organic ligands and, hence, the optical quality of the QDs. For the CdSe/14CdS QDs, 27% (partially in trap emission) of the PL

remained after Si₃N₄ deposition at 120 °C (see Figure 1(b)), whereas only 19% remained after Si₃N₄ deposition at 300 °C. The effect was more dramatic for smaller ZnS passivated CdSe QDs, where 49% of the PL was recovered after deposition at 120 °C, whereas only 7% remained at 300 °C (see Figure 1(c)). To highlight the versatility of our fabrication technique, Figure 1(d) shows that it can be extended to near-infrared emitting PbS/CdS QDs.¹⁹ The resulting Si₃N₄ layer deposited at 120 °C is less dense, as inferred from the lower refractive index of 1.85 ($\lambda = 650$ nm). Figure 1(f) shows a SEM picture of the resulting microdisk (diameter 6.0 μ m).

The spectrally and spatially resolved microphotoluminescence setup used for characterizing our devices (see Figure 1(e)) consists of a pulsed picosecond laser (100 ps pulsewidth, maximum pulse peak output power of 1 W, repetition rate between 1 kHz–1 MHz) producing a beam ($\lambda = 445$ nm) that is expanded and spatially modulated by a digital micromirror device (DMD). The micromirror plane is imaged onto the sample plane using an achromatic doublet and an objective lens (100 \times). This arrangement enables us to control the shape and the size of the excitation spot with a spatial resolution of one micrometer. The emission is collected using the same objective, separated from the excitation light with a dichroic filter, polarized using a Glan-Thompson polarizer, and sent to the slit of an imaging spectrograph. An electron multiplying charged coupled device (EMCCD) camera in the output plane of the spectrograph therefore yields spatial resolution along one dimension and spectral resolution along the other. The sample is mounted with a 10° angle between the substrate and the setup's optical axis, since the radiation pattern from WGMs is directed preferentially in a plane with a 10° angle between the substrate.²⁰

Figure 2(a) shows a transverse-electrical-polarized (TE, i.e., $\mathbf{E} \sim E_r \mathbf{e}_r$) mode map collected from a 6.0 μ m diameter microdisk. We position the sample in such a way that the slit of the imaging spectrograph takes a spatial cross section through the middle of the disk (see the drawing at the top of Figure 2(a)). This is plotted on the x-axis. The spectrograph grating then images the slit, spectrally separated along the direction perpendicular to the slit onto the EMCCD. In this way, of each point of the microdisk cross section, a spectrum is taken and plotted on the y-axis.

We pump with a spot size of 1.5 μ m, which we carefully direct at the right side of the microdisk. The PL of the excitation spot lights up, together with a bright spot of PL at the left side of the microdisk. This secondary PL spot is well out of the range of the excitation spot, since moving the excitation spot towards the left reduces rather than increases the brightness of the left spot. Hence, it cannot be attributed to direct excitation of the QDs by the pump spot. As the distance between the right edge of the excitation spot and the left spot is equal to the diameter of the disk (see Figure 2(a)), it suggests that the secondary PL spot on the left side comes from WGMs, resonating in the microdisk.

That the PL indeed comes from WGMs becomes even clearer when we take a look at a line section through the spectral mode map at the left edge (see Figure 2(b)). The spectrum exhibits some clearly distinguishable resonances, both in TE and TM (transverse magnetic) polarization, illustrating the modified density of optical modes the QDs can

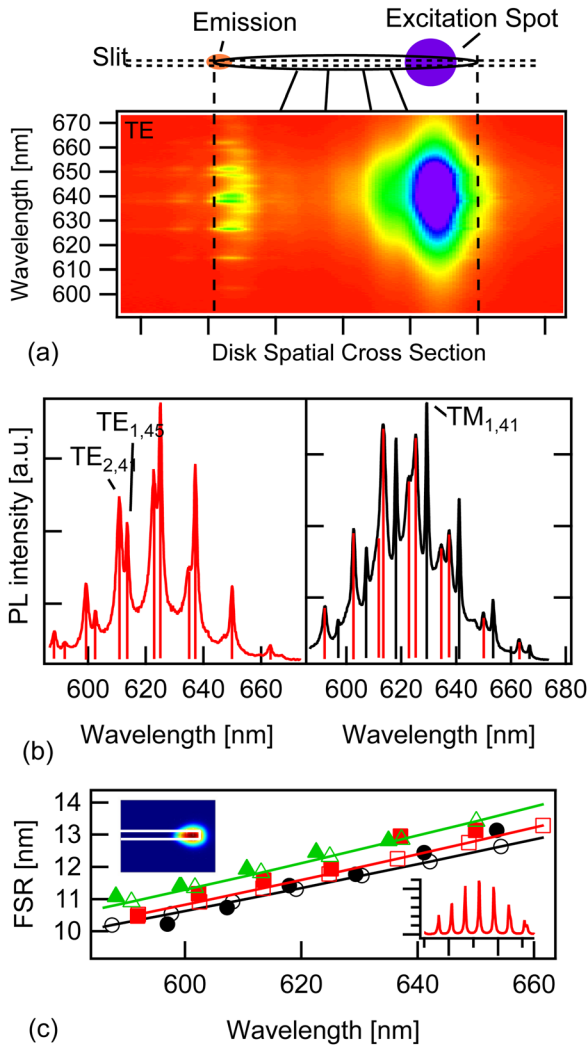


FIG. 2. (a) Mode map collected from a $6.0\ \mu\text{m}$ microdisk containing *giant* CdSe/14CdS QDs by selective excitation of the right side of the disk. The line section from where the PL is collected is drawn in the microdisk drawing above. Only TE polarized light is collected here. (b) Spectrum at the left edge of the microdisk for TE and TM polarized light. The two quasi-TE modes are also visible in the TM spectrum, as indicated by the red lines. The mode's radial and azimuthal order is indicated for one of the resonances. (c) FSR as measured (full symbols) and as calculated (open symbols) as a function of the resonance wavelength for the first order quasi-TM (black circles), first order quasi-TE (red squares), and second order quasi-TE (green triangles) mode. The inset at the top left shows the intensity mode profile of the $\text{TE}_{1,45}$ calculated using COMSOL. The inset at the bottom right shows the calculated TE spectrum, using a 1 nm linewidth.

couple to, once they are embedded in the optical cavity (see Figures 2(a) and 2(b)). Given the small excitation spot size and the low pump fluence used, we can therefore conclude that the emission coming from the left side of the microdisk is the spontaneous emission of the excited QDs on the right side of the microdisk that is coupled to a resonant microdisk mode and eventually leaks or scatters away from the disk into the collection optics.

Two WGM families stand out in the TE spectrum. They have slightly different free spectral range (FSR), indicating a different radial order (TE_1 , TE_2). In the TM spectrum three sets of modes are visible, of which only the one dominant mode is quasi-TM. We identify the other WGMs as the same quasi-TE modes seen in the TE spectrum, given that the wavelengths match with the peak positions of the quasi-TE modes.

To compare our mode mapping results with simulations, we solve the axisymmetric form of Maxwell's equations in cylindrical coordinates numerically.²¹ As illustrated in Figure 2(c), using the dimensions and refractive indices as mentioned above, we can predict the spectral positions and the FSR of the resonances for the first order quasi-TM and the first and second order quasi-TE modes within the emission band of the QDs. For the QD layer, we have taken a refractive index of 1.69 to obtain the best fit with our experimental results. A perfect match between simulations and experiment is not possible, since we neglect the QD and other material dispersion and approximate the shape of the disk cross section with a rectangle.

To understand why the quasi-TE modes show up in the TM spectrum (see Figure 2(b)), we look at the field line plots ($\mathbf{E}_t = E_r\mathbf{e}_r + E_z\mathbf{e}_z$) of the TE_1 , TE_2 , and TM_1 modes from simulations (see Figure 3). Because of the asymmetry of the microdisk structure, the TE and TM modes are hybrid. The TE modes have a non-negligible E_z component at the corners of the disk cross section. The same goes for the E_r

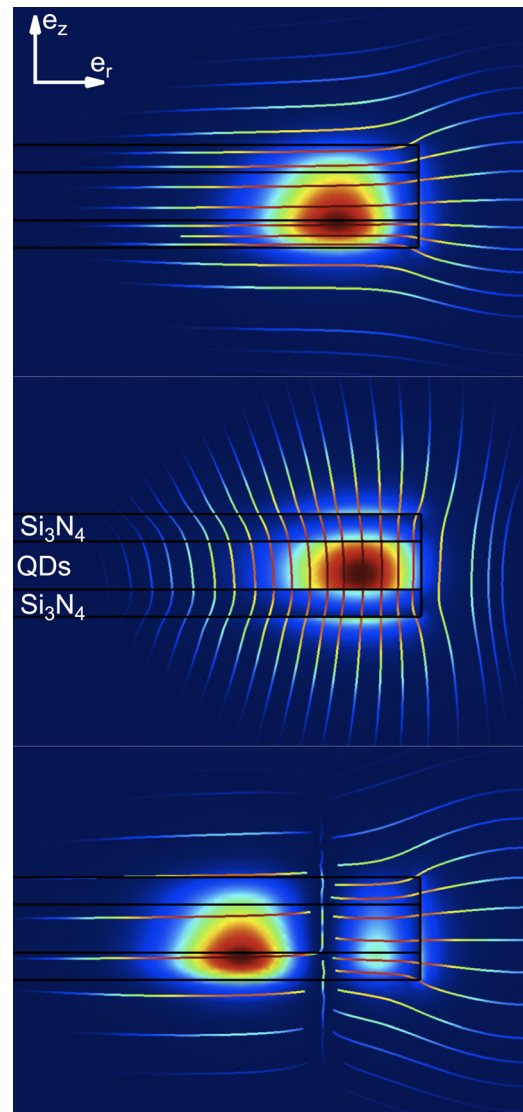


FIG. 3. Field lines $\mathbf{E}_t = E_r\mathbf{e}_r + E_z\mathbf{e}_z$ for the TE_1 (top), TM_1 (middle), and TE_2 (bottom) modes, plotted against the background of the mode intensity $|\mathbf{E}|^2$, show that both modes are hybrid, especially at the corners of the structure.

component of the TM mode at the corners, and along the top surface of the disk. Scattering of the quasi-TE modes at the microdisk corner would therefore couple to an almost pure TEM free space mode.

That scattering is the main mechanism coupling photons out of the microdisk cavity is further confirmed by the very localized spot of WGM-modulated PL, coming from the left edge of the microdisk (see Figure 2(a)). Other non-radiative loss mechanisms, such as reabsorption and Stokes-shifted re-emission outside the WGM resonance by the QDs (see Figure 1(b)) will further reduce the Q-factor of the cavity. A Lorentzian fit to the quasi-TM peaks yields Q-factors of 600, while the peaks in the TE spectrum yield Q-factors of 450 and 300 for the first and the second order modes, respectively.

Since we only pump a small part of the microdisk and keep the flux below one exciton per QD, it might seem surprising that light resonates in the microdisk at wavelengths where it is absorbed by the QDs. Even without exact knowledge of the local field factor in these densely packed QD layers,²² we can still estimate the absorption coefficient between a lower limit of 40 and an upper limit of 2000 cm⁻¹ (taking the confinement factor into account). This puts the expected Q-factors in the range of 5000–100, in agreement with our experimental results.

Both loss mechanisms could be engineered to improve the Q-factor for the desired applications. However, our main aim was to showcase embedding colloidal QDs into a CMOS-compatible solid matrix and putting them to work in an active and complex, integrated photonic device. While the photophysics of the interaction between the QD and the optical microcavity are interesting in their own right and merit further study, this work smoothes the path towards other active photonic structures, such as waveguides, ring resonators and interferometers, and more complex active photonic circuits.

In short, we have presented a platform technology to embed colloidal QDs into Si₃N₄, a standard CMOS material, for optimal stability of the QDs and improved interaction of the optical modes with the QD material. As a demonstrator, we have presented an active hybrid QD/Si₃N₄ free standing microdisk, where the spontaneous emission of the QDs is efficiently coupled to the resonant WGMs in the microdisk. Using a unique spatially and spectrally resolved micro-PL setup we are able to map the emission from the microdisk.

We identified three different families of modes and showed good agreement with simulations. This work opens the field to different and more complex active photonic circuits, using colloidal QDs.

This project was funded by the Belgian Science Policy Office (IAP P6/10), by the Fonds de la Recherche Scientifique - FNRS (F.R.S.-FNRS, Belgium) under the FRFC Grant No. 2.4.638.09F, and by the EU through the FP7 ITN network HERODOT and the ERC-project ULPPIC.

- ¹G. Schmid, *Nanoparticles: From Theory to Application* (Wiley-VCH, 2011).
- ²N. Le Thomas, U. Woggon, O. Schops, M. Artemyev, M. Kazes, and U. Banin, *Nano Lett.* **6**, 557 (2006).
- ³M. De Vittorio, F. Pisanello, L. Martiradonna, A. Quattieri, T. Stomeo, A. Bramati, and R. Cingolani, *Opto-Electron. Rev.* **18**, 1 (2010).
- ⁴S. Hoogland, V. Sukhovatkin, I. Howard, S. Cauchi, L. Levina, and E. Sargent, *Opt. Express* **14**, 3273 (2006).
- ⁵Y. Chan, J. Steckel, P. Snee, J. Caruge, J. Hodgkiss, D. Nocera, and M. Bawendi, *Appl. Phys. Lett.* **86**, 073102 (2005).
- ⁶H. Eisler, V. Sundar, M. Bawendi, M. Walsh, H. Smith, and V. Klimov, *Appl. Phys. Lett.* **80**, 4614 (2002).
- ⁷B. Moller, U. Woggon, and M. Artemyev, *Opt. Lett.* **30**, 2116 (2005).
- ⁸U. Woggon, R. Wannemacher, M. Artemyev, B. Möller, N. Le Thomas, V. Anikeyev, and O. Schöps, *Appl. Phys. B: Lasers Opt.* **77**, 469 (2003).
- ⁹A. Malko, A. Mikhailovsky, M. Petruska, J. Hollingsworth, H. Htoon, M. Bawendi, and V. Klimov, *Appl. Phys. Lett.* **81**, 1303 (2002).
- ¹⁰Y. Chan, J. Caruge, P. Snee, and M. Bawendi, *Appl. Phys. Lett.* **85**, 2460 (2004).
- ¹¹J. Schaefer, J. P. Mondia, R. Sharma, Z. H. Lu, A. S. Susha, A. L. Rogach, and L. J. Wang, *Nano Lett.* **8**, 1709 (2008).
- ¹²M. Artemyev and U. Woggon, *Appl. Phys. Lett.* **76**, 1353 (2000).
- ¹³B. Min, S. Kim, K. Okamoto, L. Yang, A. Scherer, H. Atwater, and K. Vahala, *Appl. Phys. Lett.* **89**, 191124 (2006).
- ¹⁴A. G. Pattantyus-Abraham, H. Qiao, J. Shan, K. A. Abel, T.-S. Wang, F. C. J. M. van Veggel, and J. F. Young, *Nano Lett.* **9**, 2849 (2009).
- ¹⁵X. Fan, M. C. Lonergan, Y. Zhang, and H. Wang, *Phys. Rev. B* **64**, 115310 (2001).
- ¹⁶N. Giebink, G. Wiederrecht, and M. Wasielewski, *Appl. Phys. Lett.* **98**, 081103 (2011).
- ¹⁷T. S. Luk, S. Xiong, W. W. Chow, X. Miao, G. Subramania, P. J. Resnick, A. J. Fischer, and J. C. Brinker, *J. Opt. Soc. Am. B* **28**, 1365 (2011).
- ¹⁸Y. Chen, J. Vela, H. Htoon, J. L. Casson, D. J. Werder, D. A. Bussian, V. I. Klimov, and J. A. Hollingsworth, *J. Am. Chem. Soc.* **130**, 5026 (2008).
- ¹⁹J. Pietryga, D. Werder, D. Williams, J. Casson, R. Schaller, V. Klimov, and J. Hollingsworth, *J. Am. Chem. Soc.* **130**, 4879 (2008).
- ²⁰E. Peter, A. Dousse, P. Voisin, A. Lemaître, D. Martrou, A. Cavanna, J. Bloch, and P. Senellart, *Appl. Phys. Lett.* **91**, 151103 (2007).
- ²¹M. Oxborrow, *Proc. SPIE* **6452**, 64520J (2007).
- ²²Z. Hens and I. Moreels, *J. Mater. Chem.* **22**, 10406 (2012).
- ²³See supplementary material at <http://dx.doi.org/10.1063/1.4758990> for results of microdisk devices with embedded CdSe/CdS quantum dot-in-rods.